Nucleon resonances in $\gamma p \to K^{*+}\Lambda$

A. C. Wang,[1] W. L. Wang,[2,3] F. Huang,[1,*] H. Haberzettl,[4] and K. Nakayama[3]

[1]*School of Physical Sciences, University of Chinese Academy of Sciences, Beijing 101408, China*
[2]*School of Physics and Nuclear Energy Engineering, Beihang University, Beijing 100191, China*
[3]*Department of Physics and Astronomy, University of Georgia, Athens, Georgia 30602, USA*
[4]*Institute for Nuclear Studies and Department of Physics, George Washington University, Washington, DC 20052, USA*

The high-precision cross section data for the reaction $\gamma p \to K^{*+}\Lambda$ reported by the CLAS Collaboration at the Thomas Jefferson National Accelerator Facility have been analyzed based on an effective Lagrangian approach in the tree-level approximation. Apart from the t-channel K, κ, K^* exchanges, the s-channel nucleon (N) exchange, the u-channel Λ, Σ, $\Sigma^*(1385)$ exchanges, and the generalized contact term, the contributions from the near-threshold nucleon resonances in the s channel are also taken into account in constructing the reaction amplitude. It is found that to achieve a satisfactory description of the differential cross section data, at least two nucleon resonances should be included. By including the $N(2060)5/2^-$ resonance, which is responsible for the shape of the angular distribution near the $K^*\Lambda$ threshold, and one of the $N(2000)5/2^+$, $N(2040)3/2^+$, $N(2100)1/2^+$, $N(2120)3/2^-$ and $N(2190)7/2^-$ resonances, one can describe the cross section data quite well, with the fitted resonance masses and widths compatible with those advocated by the Particle Data Group. The resulted predictions of the beam, target, and recoil asymmetries are found to be quite different from various fits, indicating the necessity of the spin observable data for $\gamma p \to K^{*+}\Lambda$ to further pin down the resonance contents and associated parameters in this reaction.

I. INTRODUCTION

The extraction of nucleon resonances (N^*'s) from experimental data and understanding their nature are essential to get insight into the nonperturbative regime of quantum chromodynamics (QCD). Our current knowledge of most of the N^*'s is mainly coming from the analyses of πN scattering and π photoproduction off the nucleon. One of the problems with this situation is that the quark models [1–3] predict the existence of many more resonances than found in these reactions. This is known as the *missing resonance problem* [4]. The number of baryon resonances in the lattice QCD calculations [5,6] is also increasing.

Some of the nucleon resonances are known to couple weakly to the πN channel, escaping detection in these reactions. This forces us to search for those missing resonances in channels other than πN, where they couple more strongly so that they can be better established. In the present work, we investigate the $K^*\Lambda$ photoproduction reaction in search for clear evidence of resonances that may be revealed through their couplings to the $K^*\Lambda$ channel. There are many attractive features in studying this reaction. First of all, resonances with sizable hidden $s\bar{s}$ content can have a better chance to be revealed in this reaction than in π production reactions. Also, since the threshold of $K^*\Lambda$ is much higher than that of πN, the $K^*\Lambda$ photoproduction off nucleons is more suited than the π production reactions for investigating the nucleon resonances in a less-explored higher N^* mass region. Another advantage of $K^*\Lambda$ photoproduction in studying N^*'s is that it acts as an "isospin filter," isolating the N^*'s with isospin $I = 1/2$.

Experimentally, so far the available data for the reaction $\gamma p \to K^{*+}\Lambda$ have all been reported by the CLAS Collaboration at the Thomas Jefferson National Accelerator Facility (JLab). The first preliminary total cross section data for center-of-mass energy, W, from threshold up to 2.85 GeV were reported by Guo *et al.* in 2006 in a conference proceedings [7]. Later, the preliminary differential cross section data for this reaction from $W = 2.22$ to 2.42 GeV were reported by Hicks *et al.* in 2011 in another conference proceedings [8]. It was only in 2013 that the first high-statistics cross section data for this reaction were published by Tang *et al.* in Ref. [9], where the measured differential cross sections and the extracted total cross sections are presented from threshold up to $W \approx 2.85$ GeV. Also, some preliminary differential cross section data for the $\gamma n \to K^{*0}\Lambda$ reaction have been reported by Mattione in a conference proceedings [10].

The CLAS differential cross section data for $\gamma p \to K^{*+}\Lambda$ [9] show some structures near the $K^{*+}\Lambda$ threshold energy which may indicate some possible contribution from nucleon resonance(s). In fact, in this energy region, there are six resonances advocated in the most recent Particle Data Group (PDG) review [11] that might potentially contribute to this reaction, namely, $N(2000)5/2^+$, $N(2040)3/2^+$, $N(2060)5/2^-$, $N(2100)1/2^+$, $N(2120)3/2^-$, and $N(2190)7/2^-$. Among them, $N(2190)7/2^-$ is rated as a four-star resonance but with rather broad mass (2100–2200 MeV) and width (300–700 MeV); $N(2000)5/2^+$, $N(2060)5/2^-$, and $N(2120)3/2^-$ are rated as two-star resonances and $N(2040)3/2^+$ and $N(2100)1/2^+$ as one-star resonances. This means that the four-star $N(2190)7/2^-$ resonance needs further investigation to improve the accuracy of its parameters, and the other five two- and one-star resonances need more information, especially from the reaction channels (other than those cited

———————
*Corresponding author: huangfei@ucas.edu.cn

by PDG) to which these resonances couple more strongly, to improve the evidences of their existences and to extract their parameters. The high-statistics cross section data for $\gamma p \to K^{*+}\Lambda$ from the CLAS Collaboration [9] promote the studies along this direction.

Theoretically, several works based on effective Lagrangian approaches have already been devoted to the study of $K^*\Lambda$ photoproduction reaction [12–14,17–19]. In 2006, Oh and Kim investigated the nonresonant contributions for $\gamma N \to K^*\Lambda$ within an isobar model, and they found that the t-channel K exchange, which causes a sharp raise of the differential cross sections at forward-scattering angles, dominates this reaction process [12]. Further, in late 2006, they examined the contribution of scalar meson κ and concluded that the t-channel κ exchange in $\gamma p \to K^{*+}\Lambda$ is rather small [13]. In 2010, Ozaki *et al.* studied the $\gamma p \to K^{*+}\Lambda$ reaction in a Regge model [14]. They obtained the total cross sections compatible with CLAS's preliminary data [7] and found that the contributions from the K^* trajectory and reggeized contact term are much bigger than those in the isobar model of Ref. [12]. (However, we point out here that the Regge model of Ref. [15] used in Ref. [14] is based on incorrect dynamical assumptions, as shown in Ref. [16].) In 2011, Kim *et al.* [17] have included the contributions from the resonances $N(2080)3/2^-$ and $N(2200)5/2^-$ based on the theoretical models of Refs. [12,13] in order to describe the preliminary differential cross section data from CLAS [8]. They have found that the nonresonant contributions dominate the $K^*\Lambda$ photoproduction reaction, while the resonance $N(2080)3/2^-$ plays a crucial role in explaining the enhancement of the near-threshold production rate; the contribution from $N(2200)5/2^-$ is rather small. When the first high-statistics cross section data from CLAS were published in 2013 [9], it was found that all mentioned theoretical calculations [12–14,17] significantly underestimate the cross sections in the range of (laboratory) photon energy of 2.1 GeV $< E_\gamma < 3.1$ GeV. Then, in 2014, Kim *et al.* reinvestigated [18] the $K^*\Lambda$ photoproduction reaction to accommodate the most recent CLAS data [9]. They considered four nucleon resonances, namely $N(2000)5/2^+$, $N(2060)5/2^-$, $N(2120)3/2^-$, and $N(2190)7/2^-$, in addition to the nonresonant contributions as included in Ref. [17], and found that apart from the significant contributions from the t-channel K and κ exchanges, the s-channel nucleon resonances $N(2120)3/2^-$ and $N(2190)7/2^-$ play very important roles in reproducing the experimental cross section data. The contribution from the resonance $N(2060)5/2^-$ was found to be small but noticeable, while that from $N(2000)5/2^+$ was found to be almost negligible. In Ref. [19], the total cross sections and the differential cross sections at three selected energies for $\gamma N \to K^*\Lambda$ are investigated within a Regge approach. (The dynamical assumptions [15] of this Regge analysis are also marred by incomplete dynamical assumptions [16].) It is found that the K and K^* trajectories dominate the the process of $K^{*+}\Lambda$ photoproduction. The preliminary differential cross section data for $\gamma n \to K^{*0}\Lambda$ [10] have been also analyzed recently by Wang and He [20] in an effective Lagrangian approach.

The work of Ref. [18] presents so far the only detailed theoretical analysis of the most recent high-statistics differential cross section data for $\gamma p \to K^{*+}\Lambda$ reported by

the CLAS Collaboration [9]. It describes the total cross section data quite well in the photon energy region of $E_\gamma < 3.5$ GeV, and the differential cross section data have also been qualitatively described. Nevertheless, there is still some room for improvement in their results for the differential cross sections, especially, near the $K^{*+}\Lambda$ threshold, where the nucleon resonances are relevant. Figure 1 illustrates this issue; there, a comparison of the differential cross sections from the theoretical calculation of Ref. [18] (blue dashed lines) with the most recent CLAS data [9] (scattered symbols) at some selected energies in the near-threshold region is shown. The numbers in parentheses denote the photon laboratory incident energy, E_γ (left number), and the total center-of-mass energy of the system, W (right number). The black solid lines represent the results from model I of our present work, which will be discussed in detail in Sec. III. It is clearly seen from Fig. 1 that there is still some room for improvement in the differential cross section results of Ref. [18]. We mention that in Ref. [18] the resonance parameters of $N(2000)5/2^+$ and $N(2060)5/2^-$ are taken from Ref. [21], the parameters of $N(2190)7/2^-$ are taken from Ref. [22], and the parameters of $N(2120)3/2^-$ are determined by a fit to the experimental data.

In this work, we investigate the $\gamma p \to K^{*+}\Lambda$ reaction based on an effective Lagrangian approach in the tree-level approximation. We expect that a better description of the data for this reaction will allow for a more reliable extraction of the resonance content and their associated parameters. One of the major differences of our theoretical model compared with that of Refs. [17,18] is that in the latter a common form factor is introduced in the reaction amplitudes in order to preserve gauge invariance, while in our work, following Refs. [23–26], a generalized contact current—that accounts effectively for the interaction current arising from the unknown parts of the underlying microscopic model—is introduced in such a way that the full photoproduction amplitude satisfies the generalized Ward-Takahashi identity (WTI) and thus it is fully gauge invariant. As a consequence, our model is free from such an artificial constraint as the use of a common form factor. Moreover, and most relevantly, we adopt a rather different strategy in choosing the nucleon resonances to be considered in our model. Instead of including all of them, we introduce the nucleon resonances in the present work as few as possible with the resonance parameters being adjusted to reproduce the data. We find that apart from the t-channel K, κ, K^* exchanges, the s-channel nucleon (N) exchange, the u-channel $\Lambda, \Sigma, \Sigma^*(1385)$ exchanges, and the generalized contact current, at least two nucleon resonances near the $K^*\Lambda$ threshold should be included in the s channel in order to obtain a satisfactory description of the CLAS high-statistics differential cross section data. By including the $N(2060)5/2^-$ resonance, which, as we shall show later, is responsible for the shape of the angular distribution near the $K^*\Lambda$ threshold, and one of the $N(2000)5/2^+$, $N(2040)3/2^+$, $N(2100)1/2^+$, $N(2120)3/2^-$, and $N(2190)7/2^-$ resonances, we get five fits with roughly similar fit qualities. The resulting differential and total cross sections are both in very good agreement overall with the most recent CLAS data [9]. In particular, the angular dependence of the differential cross sections near the $K^{*+}\Lambda$ threshold is now, for the first
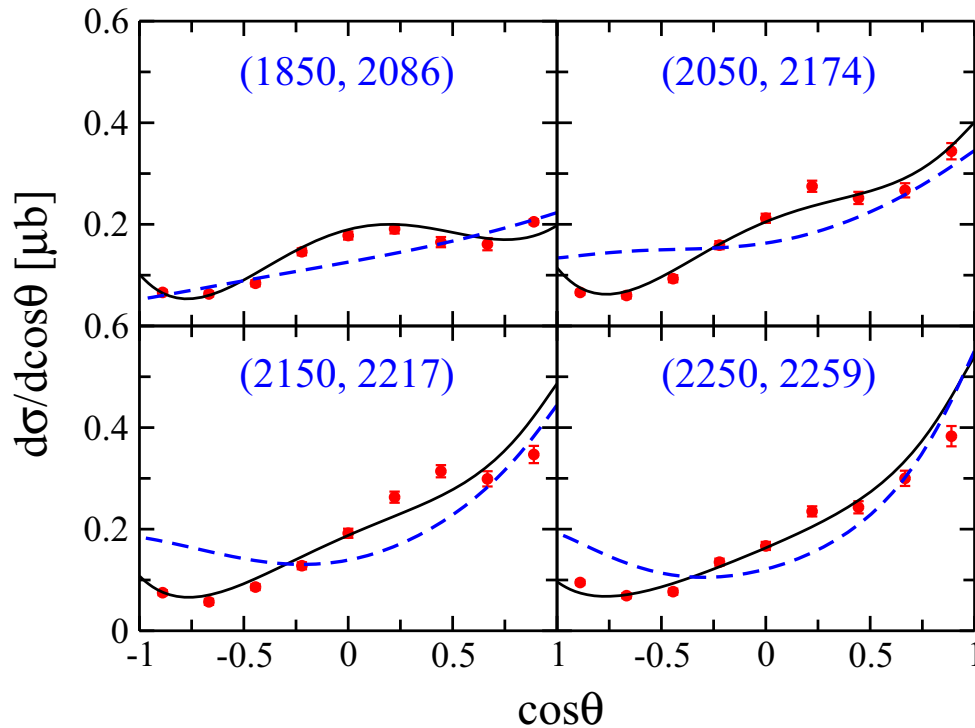
FIG. 1. Status of theoretical description of the differential cross sections for $\gamma p \rightarrow K^{*+}\Lambda$ at selected energies in the near-threshold region. The numbers in parentheses denote the photon laboratory incident energy (left number) and the total center-of-mass energy of the system (right number). The blue dashed lines represent the results from Ref. [18], and the black solid lines denote the results from model I of our present work, which will be discussed later. The scattered symbols are the most recent data from CLAS Collaboration [9].

time, described quite well. The fitted resonance masses and widths are compatible with those advocated by the PDG [11]. The nonresonant terms, dominated by the t-channel K exchange, are found to have very significant contributions. The predictions for the photon beam asymmetry, target nucleon asymmetry, and recoil Λ asymmetry are also given; they are found to be more sensitive to the details of the model than the cross sections, indicating the necessity of data on these spin observables to further constrain the resonance contents and their parameters in this reaction.

Of course, a more complete analysis and extraction of nucleon resonances requires a coupled-channels approach [27–31], so far developed mostly for pseudoscalar meson production reactions. In this approach, the unitarity and analyticity of the reaction amplitude can be maintained and the search of poles (associated with the resonances) in the complex energy plane can be performed. This is beyond the scope of the present work, which may be considered as a first step toward developing such a more complete model.

The present paper is organized as follows. In Sec. II, we briefly introduce the framework of our theoretical model. There, the strategy for imposing gauge invariance of the photoproduction amplitude according to the generalized WTI, the specific forms of the effective interaction Lagrangians, the resonance propagators, and the phenomenological form factors are explicitly presented. In Sec. III, the results of our model calculations are shown, including a comparison of our calculated cross sections with the most recent high-statistics

CLAS data, an analysis of the $\gamma p \rightarrow K^{*+}\Lambda$ reaction dynamics, and a discussion of the resulting resonance contents and associated parameters. Our predicted beam, target, and recoil asymmetries in $\gamma p \rightarrow K^{*+}\Lambda$ are also shown and discussed in this section. Finally a brief summary and conclusions are given in Sec. IV.

II. FORMALISM

Following a full field theoretical approach of Refs. [23–26], the full reaction amplitude for $\gamma N \rightarrow K^*\Lambda$ can be expressed as

$$M^{\nu\mu} = M_s^{\nu\mu} + M_t^{\nu\mu} + M_u^{\nu\mu} + M_{\text{int}}^{\nu\mu}, \qquad (1)$$

with ν and μ being the Lorentz indices of vector meson K^* and photon γ, respectively. The first three terms $M_s^{\nu\mu}$, $M_t^{\nu\mu}$, and $M_u^{\nu\mu}$ stand for the s-, t-, and u-channel pole diagrams, respectively, with s, t, and u being the Mandelstam variables of the internally exchanged particles. They arise from the photon attaching to the external particles in the underlying $\Lambda N K^*$ interaction vertex. The last term, $M_{\text{int}}^{\nu\mu}$, stands for the interaction current which arises from the photon attaching to the internal structure of the $\Lambda N K^*$ interaction vertex. All four terms in Eq. (1) are diagrammatically depicted in Fig. 2.

In the present work, the following contributions, as shown in Fig. 2, are considered in constructing the s-, t-, and u-channel amplitudes: (a) N and N^*'s exchanges in the s channel, (b) K, κ, and K^* meson exchanges in the t channel, and
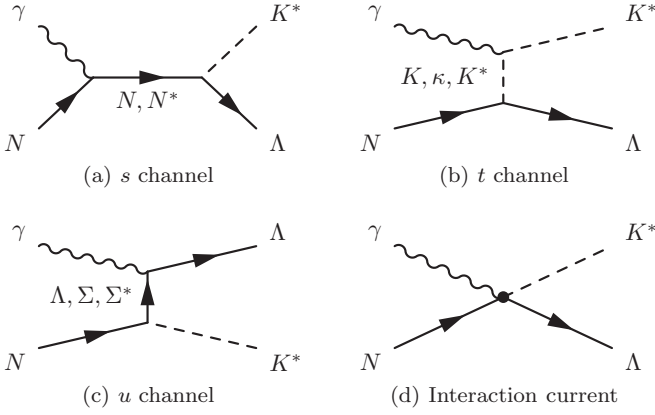
FIG. 2. Generic structure of the K^* photoproduction amplitude for $\gamma N \to K^* \Lambda$. Time proceeds from left to right.

(c) Λ, Σ, and $\Sigma^*(1385)$ hyperon exchanges in the u channel. The exchanges of other hyperon resonances with higher masses in the u channel are tested to have tiny contributions and thus are omitted in the present work in order to reduce the model parameters. Using an effective Lagrangian approach, one can, in principle, obtain explicit expressions for these amplitudes. However, the exact calculation of the interaction current $M_{\text{int}}^{\nu\mu}$ is impractical, as it obeys a highly nonlinear equation and contains diagrams with very complicated interaction dynamics. Furthermore, the introduction of phenomenological form factors makes it impossible to calculate the interaction current exactly even in principle. Following Refs. [23–25], we model the interaction current by a generalized contact current,

$$M_{\text{int}}^{\nu\mu} = \Gamma_{\Lambda N K^*}^{\nu}(q) C^{\mu} + M_{\text{KR}}^{\nu\mu} f_t. \quad (2)$$

Here $\Gamma_{\Lambda N K^*}^{\nu}(q)$ is the vertex function of $\Lambda N K^*$ coupling given by the Lagrangian of Eq. (21),

$$\Gamma_{\Lambda N K^*}^{\nu}(q) = -i g_{\Lambda N K^*}\left[\gamma^{\nu} - i\frac{\kappa_{\Lambda N K^*}}{2M_N}\sigma^{\nu\alpha}q_{\alpha}\right], \quad (3)$$

with q being the 4-momentum of the outgoing K^* meson; $M_{\text{KR}}^{\nu\mu}$ is the Kroll-Ruderman term given by the Lagrangian of Eq. (35),

$$M_{\text{KR}}^{\nu\mu} = g_{\Lambda N K^*}\frac{\kappa_{\Lambda N K^*}}{2M_N}\sigma^{\nu\mu}Q_{K^*}, \quad (4)$$

with Q_{K^*} being the electric charge of K^*; f_t in Eq. (2) is the phenomenological form factor attached to the amplitude of t-channel K^* exchange, which is given in Eq. (43); and C^{μ} is an auxiliary current, which is nonsingular, introduced to ensure that the full photoproduction amplitude of Eq. (1) satisfies the generalized WTI and thus is fully gauge invariant. Following Refs. [24,25], we choose C^{μ} for $\gamma p \to K^{*+}\Lambda$ as

$$C^{\mu} = -Q_{K^*}\frac{f_t - \hat{F}}{t - q^2}(2q - k)^{\mu} - Q_N\frac{f_s - \hat{F}}{s - p^2}(2p + k)^{\mu}, \quad (5)$$

with

$$\hat{F} = 1 - \hat{h}(1 - f_s)(1 - f_t). \quad (6)$$

Here p, q, and k are 4-momenta of the incoming N, outgoing K^*, and the incoming photon, respectively; $Q_{N(K^*)}$ is the

electric charge of $N(K^*)$; f_s is the phenomenological form factor for s-channel N exchange. $\hat{h}$ is an arbitrary function, except that it should go to unity in the high-energy limit to prevent the "violation of scaling behavior" [32]. For the sake of simplicity, in the present work it is taken to be $\hat{h} = 1$.

In the rest of this section, we present the effective Lagrangians, the resonance propagators, and the phenomenological form factors employed in the present work.

A. Effective Lagrangians

The effective interaction Lagrangians used in the present work for the production amplitudes are given below. For further convenience, we define the operators

$$\Gamma^{(+)} = \gamma_5 \quad \text{and} \quad \Gamma^{(-)} = 1, \quad (7)$$

and the field-strength tensors

$$K^{*\mu\nu} = \partial^{\mu}K^{*\nu} - \partial^{\nu}K^{*\mu}, \quad (8)$$

$$F^{\mu\nu} = \partial^{\mu}A^{\nu} - \partial^{\nu}A^{\mu}, \quad (9)$$

with $K^{*\mu}$ and A^{μ} denoting the K^* vector-meson field and electromagnetic field, respectively.

The electromagnetic interaction Lagrangians required to calculate the nonresonant Feynman diagrams are

$$\mathcal{L}_{NN\gamma} = -e\bar{N}\left[\left(\hat{e}\gamma^{\mu} - \frac{\hat{\kappa}_N}{2M_N}\sigma^{\mu\nu}\partial_{\nu}\right)A_{\mu}\right]N, \quad (10)$$

$$\mathcal{L}_{\gamma K^* K^*} = -e(K^{*\nu} \times K_{\mu\nu}^*)_3 A^{\mu}, \quad (11)$$

$$\mathcal{L}_{\gamma \kappa K^*} = e\frac{g_{\gamma \kappa K^*}}{2M_{K^*}}F^{\mu\nu}K_{\mu\nu}^*\kappa, \quad (12)$$

$$\mathcal{L}_{\gamma K K^*} = e\frac{g_{\gamma K K^*}}{M_K}\varepsilon^{\alpha\mu\lambda\nu}(\partial_{\alpha}A_{\mu})(\partial_{\lambda}K)K_{\nu}^*, \quad (13)$$

$$\mathcal{L}_{\Lambda\Lambda\gamma} = e\frac{\kappa_{\Lambda}}{2M_N}\bar{\Lambda}\sigma^{\mu\nu}(\partial_{\nu}A_{\mu})\Lambda, \quad (14)$$

$$\mathcal{L}_{\Sigma\Lambda\gamma} = e\frac{\kappa_{\Sigma\Lambda}}{2M_N}\bar{\Lambda}\sigma^{\mu\nu}(\partial_{\nu}A_{\mu})\Sigma^0 + \text{H. c.}, \quad (15)$$

$$\mathcal{L}_{\Sigma^*\Lambda\gamma} = ie\frac{g_{\Sigma^*\Lambda\gamma}^{(1)}}{2M_N}\bar{\Lambda}\gamma_{\nu}\gamma_5 F^{\mu\nu}\Sigma_{\mu}^{*0}$$
$$- e\frac{g_{\Sigma^*\Lambda\gamma}^{(2)}}{(2M_N)^2}(\partial_{\nu}\bar{\Lambda})\gamma_5 F^{\mu\nu}\Sigma_{\mu}^{*0} + \text{H. c.}, \quad (16)$$

where e is the elementary charge unit and $\hat{e}$ stands for the charge operator; $\hat{\kappa}_N = \kappa_p(1 + \tau_3)/2 + \kappa_n(1 - \tau_3)/2$, with the anomalous magnetic moments $\kappa_p = 1.793$ and $\kappa_n = -1.913$; $\kappa_{\Lambda} = -0.613$ is the Λ anomalous magnetic moment and $\kappa_{\Sigma\Lambda} = -1.61$ is the anomalous magnetic moment for the $\Sigma^0 \to \Lambda\gamma$ transition; M_N, M_K, and M_{K^*} stand for the masses of N, K, and K^*, respectively; and $\varepsilon^{\alpha\mu\lambda\nu}$ is the totally antisymmetric Levi-Civita tensor with $\varepsilon^{0123} = 1$. The coupling constant $g_{\gamma \kappa K^*} = 0.214$ is taken from Refs. [17,18], determined by a vector-meson dominance model proposed by Black *et al.* [33]. The value of the electromagnetic coupling $g_{\gamma K K^*}$ is determined by fitting the radiative decay width of $K^* \to K\gamma$ given by the PDG [11], which leads to $g_{\gamma K^{\pm}K^{*\pm}} = 0.413$, with the sign inferred from $g_{\gamma\pi\rho}$ [34] via the flavor SU(3) symmetry considerations in conjunction with

the vector-meson dominance assumption. The electromagnetic couplings $g^{(1)}_{\Sigma^*\Lambda\gamma}$ and $g^{(2)}_{\Sigma^*\Lambda\gamma}$ should, in principle, be fixed by the helicity amplitudes of the transition reaction $\Sigma^{*0} \to \Lambda\gamma$. Nevertheless, the latest PDG [11] is still devoid of such information, and thus we treat the coupling $g^{(1)}_{\Sigma^*\Lambda\gamma}$ as a fit parameter and let the coupling $g^{(2)}_{\Sigma^*\Lambda\gamma}$ be determined by the PDG value of the partial decay width, $\Gamma_{\Sigma^{*0}\to\Lambda\gamma} = 0.45$ MeV [11].

The resonance-nucleon-photon transition Lagrangians are

$$\mathcal{L}^{1/2\pm}_{RN\gamma} = e\frac{g^{(1)}_{RN\gamma}}{2M_N}\bar{R}\Gamma^{(\mp)}\sigma_{\mu\nu}(\partial^\nu A^\mu)N + \text{H.c.}, \tag{17}$$

$$\mathcal{L}^{3/2\pm}_{RN\gamma} = -ie\frac{g^{(1)}_{RN\gamma}}{2M_N}\bar{R}_\mu\gamma_\nu\Gamma^{(\pm)}F^{\mu\nu}N$$
$$+ e\frac{g^{(2)}_{RN\gamma}}{(2M_N)^2}\bar{R}_\mu\Gamma^{(\pm)}F^{\mu\nu}\partial_\nu N + \text{H.c.}, \tag{18}$$

$$\mathcal{L}^{5/2\pm}_{RN\gamma} = e\frac{g^{(1)}_{RN\gamma}}{(2M_N)^2}\bar{R}_{\mu\alpha}\gamma_\nu\Gamma^{(\mp)}(\partial^\alpha F^{\mu\nu})N$$
$$\pm ie\frac{g^{(2)}_{RN\gamma}}{(2M_N)^3}\bar{R}_{\mu\alpha}\Gamma^{(\mp)}(\partial^\alpha F^{\mu\nu})\partial_\nu N + \text{H.c.}, \tag{19}$$

$$\mathcal{L}^{7/2\pm}_{RN\gamma} = ie\frac{g^{(1)}_{RN\gamma}}{(2M_N)^3}\bar{R}_{\mu\alpha\beta}\gamma_\nu\Gamma^{(\pm)}(\partial^\alpha\partial^\beta F^{\mu\nu})N$$
$$- e\frac{g^{(2)}_{RN\gamma}}{(2M_N)^4}\bar{R}_{\mu\alpha\beta}\Gamma^{(\pm)}(\partial^\alpha\partial^\beta F^{\mu\nu})\partial_\nu N + \text{H.c.}, \tag{20}$$

where R designates the nucleon resonance, and the superscript of $\mathcal{L}_{RN\gamma}$ denotes the spin and parity of the resonance R. The coupling constants $g^{(i)}_{RN\gamma}$ ($i = 1, 2$) are fit parameters.

The effective Lagrangians for meson-baryon interactions are

$$\mathcal{L}_{\Lambda NK^*} = -g_{\Lambda NK^*}\bar{\Lambda}\left[\left(\gamma^\mu - \frac{\kappa_{\Lambda NK^*}}{2M_N}\sigma^{\mu\nu}\partial_\nu\right)K^*_\mu\right]N + \text{H.c.}, \tag{21}$$

$$\mathcal{L}_{\Lambda N\kappa} = -g_{\Lambda N\kappa}\bar{\Lambda}\kappa N + \text{H.c.}, \tag{22}$$

$$\mathcal{L}_{\Lambda NK} = -g_{\Lambda NK}\bar{\Lambda}\Gamma^{(+)}\left[\left(i\lambda + \frac{1-\lambda}{2M_N}\slashed{\partial}\right)K\right]N + \text{H.c.}, \tag{23}$$

$$\mathcal{L}_{\Sigma NK^*} = -g_{\Sigma NK^*}\bar{\Sigma}\left[\left(\gamma^\mu - \frac{\kappa_{\Sigma NK^*}}{2M_N}\sigma^{\mu\nu}\partial_\nu\right)K^*_\mu\right]N + \text{H.c.}, \tag{24}$$

$$\mathcal{L}_{\Sigma^*NK^*} = -i\frac{g^{(1)}_{\Sigma^*NK^*}}{2M_N}\bar{\Sigma}^*_\mu\gamma_\nu\gamma_5 K^{*\mu\nu}N$$
$$+ \frac{g^{(2)}_{\Sigma^*NK^*}}{(2M_N)^2}\bar{\Sigma}^*_\mu\gamma_5 K^{*\mu\nu}\partial_\nu N$$
$$- \frac{g^{(3)}_{\Sigma^*NK^*}}{(2M_N)^2}\bar{\Sigma}^*_\mu\gamma_5(\partial_\nu K^{*\mu\nu})N + \text{H.c.}, \tag{25}$$

where the parameter λ was introduced in $\mathcal{L}_{\Lambda NK}$ to interpolate between the pseudovector ($\lambda = 0$) and the pseudoscalar ($\lambda = 1$) couplings. Unlike for the pion coupling, where the low-energy chiral perturbation theory calls for the pseudovector coupling over the pseudoscalar coupling, for kaons, the situation is much less clear. In fact, some authors have employed pseudoscalar coupling [18] and others have allowed for both types of couplings [35]. On the other hand, it is a common practice to rely on SU(3) flavor symmetry for obtaining the effective Lagrangians when studying the kaon-baryon systems, which implies a pseudovector ΛNK coupling, since the pseudovector coupling is used in the $NN\pi$ vertex as demanded by chiral symmetry. For example, Haidenbauer *et al.* [36] have obtained an excellent description of the hyperon-nucleon system in chiral effective field theory, i.e., with pseudovector ΛNK coupling. In the present work, following Refs. [29,36], λ is set to be zero; i.e., we adopt the pure pseudovector type of coupling. Although we shall not show any results with the pseudoscalar coupling for the ΛNK vertex in the present work, we just mention that we have tested this coupling type during the trial calculations and found that it leads to results that are systematically worse by a factor of ~ 1.5 in χ^2 than those obtained using the pseudovector coupling. The coupling constant $g_{\Lambda NK} = 13.99$ is taken from Ref. [29], determined by the flavor SU(3) symmetry. The coupling constants $g_{\Lambda NK^*}, \kappa_{\Lambda NK^*}, g_{\Sigma NK^*}, \kappa_{\Sigma NK^*},$ and $g^{(1)}_{\Sigma^*NK^*}$ are also fixed by the flavor SU(3) symmetry [29,37],

$$g_{\Lambda NK^*} = -\frac{1}{2\sqrt{3}}g_{NN\omega} - \frac{\sqrt{3}}{2}g_{NN\rho} = -6.21, \tag{26}$$

$$\kappa_{\Lambda NK^*} = \frac{f_{\Lambda NK^*}}{g_{\Lambda NK^*}} = -\frac{\sqrt{3}}{2}\frac{f_{NN\rho}}{g_{\Lambda NK^*}} = 2.76, \tag{27}$$

$$g_{\Sigma NK^*} = -\frac{1}{2}g_{NN\omega} + \frac{1}{2}g_{NN\rho} = -4.26, \tag{28}$$

$$\kappa_{\Sigma NK^*} = \frac{f_{\Sigma NK^*}}{g_{\Sigma NK^*}} = \frac{1}{2}\frac{f_{NN\rho}}{g_{\Sigma NK^*}} = -2.33, \tag{29}$$

$$g^{(1)}_{\Sigma^*NK^*} = -\frac{1}{\sqrt{6}}g_{\Delta N\rho} = 15.96, \tag{30}$$

where the empirical values $g_{NN\rho} = 3.25, g_{NN\omega} = 11.76, \kappa_{NN\rho} = g_{NN\rho}/f_{NN\rho} = 6.1$, and $g_{\Delta N\rho} = -39.10$ from Refs. [25,29] are used. As the $g^{(2)}$ and $g^{(3)}$ terms in the $\Delta N\rho$ interactions have never been seriously studied in literature, the corresponding couplings for the Σ^*NK^* interactions, i.e., $g^{(2)}_{\Sigma^*NK^*}$ and $g^{(3)}_{\Sigma^*NK^*}$, cannot be determined via flavor SU(3) symmetry, and we ignore these two terms in the present work, following Refs. [17,18]. The coupling constant $g_{\Lambda N\kappa} = -8.312$ is taken from Nijmegen model NSC97a [38], determined by a fit to the $\Lambda N - \Sigma N$ scattering data.

The effective Lagrangians for hadronic vertices including nucleon resonances are

$$\mathcal{L}^{1/2\pm}_{R\Lambda K^*} = -\frac{g_{R\Lambda K^*}}{2M_N}\bar{R}\Gamma^{(\mp)}\left\{\left[\left(\frac{\gamma_\mu\partial^2}{M_R \mp M_N} \pm i\partial_\mu\right)\right. \right.$$
$$\left.\left. -\frac{f_{R\Lambda K^*}}{g_{R\Lambda K^*}}\sigma_{\mu\nu}\partial^\nu\right]K^{*\mu}\right\}\Lambda + \text{H.c.}, \tag{31}$$

$$\mathcal{L}_{R\Lambda K^*}^{3/2\pm} = -i\frac{g_{R\Lambda K^*}^{(1)}}{2M_N}\bar{R}_\mu\gamma_\nu\Gamma^{(\pm)}K^{*\mu\nu}\Lambda$$

$$+ \frac{g_{R\Lambda K^*}^{(2)}}{(2M_N)^2}\bar{R}_\mu\Gamma^{(\pm)}K^{*\mu\nu}\partial_\nu\Lambda$$

$$\mp \frac{g_{R\Lambda K^*}^{(3)}}{(2M_N)^2}\bar{R}_\mu\Gamma^{(\pm)}(\partial_\nu K^{*\mu\nu})\Lambda + \text{H.c.,} \quad (32)$$

$$\mathcal{L}_{R\Lambda K^*}^{5/2\pm} = \frac{g_{R\Lambda K^*}^{(1)}}{(2M_N)^2}\bar{R}_{\mu\alpha}\gamma_\nu\Gamma^{(\mp)}(\partial^\alpha K^{*\mu\nu})\Lambda$$

$$\pm i\frac{g_{R\Lambda K^*}^{(2)}}{(2M_N)^3}\bar{R}_{\mu\alpha}\Gamma^{(\mp)}(\partial^\alpha K^{*\mu\nu})\partial_\nu\Lambda$$

$$\mp i\frac{g_{R\Lambda K^*}^{(3)}}{(2M_N)^3}\bar{R}_{\mu\alpha}\Gamma^{(\mp)}(\partial^\alpha\partial_\nu K^{*\mu\nu})\Lambda + \text{H.c.,} \quad (33)$$

$$\mathcal{L}_{R\Lambda K^*}^{7/2\pm} = i\frac{g_{R\Lambda K^*}^{(1)}}{(2M_N)^3}\bar{R}_{\mu\alpha\beta}\gamma_\nu\Gamma^{(\pm)}(\partial^\alpha\partial^\beta K^{*\mu\nu})\Lambda$$

$$- \frac{g_{R\Lambda K^*}^{(2)}}{(2M_N)^4}\bar{R}_{\mu\alpha\beta}\Gamma^{(\pm)}(\partial^\alpha\partial^\beta K^{*\mu\nu})\partial_\nu\Lambda$$

$$\pm \frac{g_{R\Lambda K^*}^{(3)}}{(2M_N)^4}\bar{R}_{\mu\alpha\beta}\Gamma^{(\pm)}(\partial^\alpha\partial^\beta\partial_\nu K^{*\mu\nu})\Lambda + \text{H.c.} \quad (34)$$

In the present work, the coupling constant $f_{R\Lambda K^*}$ in $\mathcal{L}_{R\Lambda K^*}^{1/2\pm}$ is set to be zero, and the $g_{R\Lambda K^*}^{(2)}$ and $g_{R\Lambda K^*}^{(3)}$ terms in $\mathcal{L}_{R\Lambda K^*}^{3/2\pm}$, $\mathcal{L}_{R\Lambda K^*}^{5/2\pm}$ and $\mathcal{L}_{R\Lambda K^*}^{7/2\pm}$ are ignored for the sake of simplicity. The parameters $g_{R\Lambda K^*}$ and $g_{R\Lambda K^*}^{(1)}$ are fit parameters. Actually, only the products of the electromagnetic couplings and the hadronic couplings of nucleon resonances are relevant to the reaction amplitudes, and these products are what we really fit in practice.

The effective Lagrangian for the Kroll-Ruderman term of $\gamma N \to \Lambda K^*$ reads

$$\mathcal{L}_{\gamma N\Lambda K^*} = -ig_{\Lambda N K^*}\frac{\kappa_{\Lambda N K^*}}{2M_N}\bar{\Lambda}\sigma^{\mu\nu}A_\nu\hat{Q}_{K^*}K_\mu^*N + \text{H.c.,} \quad (35)$$

with $\hat{Q}_{K^*}$ being the electric charge operator of the outgoing K^* meson. This interaction Lagrangian is obtained by the minimal gauge substitution $\partial_\mu \to \mathcal{D}_\mu \equiv \partial_\mu - i\hat{Q}_{K^*}A_\mu$ in the $\Lambda N K^*$ interaction Lagrangian of Eq. (21). The couplings $g_{\Lambda N K^*}$ and $\kappa_{\Lambda N K^*}$ have been given in Eqs. (26) and (27).

B. Resonance propagators

In principle, an energy-dependent width of resonance is more realistic than a constant value multiplied by a step function. However, as discussed in Ref. [39], the cross section data alone are usually insensitive to the energy dependence of the resonance width. For the reaction of $\gamma N \to K^*\Lambda$, so far we only have the differential cross section data while the data for spin observables are not available. Hence, it is justified to treat the resonance width as a constant instead of a complex energy-dependent function for the sake of simplicity.

For spin-1/2 resonance propagator, we use the ansatz

$$S_{1/2}(p) = \frac{i}{\not{p} - M_R + i\Gamma/2}, \quad (36)$$

where M_R and Γ are the mass and width of resonance R with four-momentum p, respectively.

Following Refs. [40–42], the prescriptions of the propagators for resonances with spin-3/2, spin-5/2, and spin-7/2 are

$$S_{3/2}(p) = \frac{i}{\not{p} - M_R + i\Gamma/2}\left(\tilde{g}_{\mu\nu} + \frac{1}{3}\tilde{\gamma}_\mu\tilde{\gamma}_\nu\right), \quad (37)$$

$$S_{5/2}(p) = \frac{i}{\not{p} - M_R + i\Gamma/2}\left[\frac{1}{2}(\tilde{g}_{\mu\alpha}\tilde{g}_{\nu\beta} + \tilde{g}_{\mu\beta}\tilde{g}_{\nu\alpha})\right.$$

$$- \frac{1}{5}\tilde{g}_{\mu\nu}\tilde{g}_{\alpha\beta} + \frac{1}{10}(\tilde{g}_{\mu\alpha}\tilde{\gamma}_\nu\tilde{\gamma}_\beta + \tilde{g}_{\mu\beta}\tilde{\gamma}_\nu\tilde{\gamma}_\alpha$$

$$\left. + \tilde{g}_{\nu\alpha}\tilde{\gamma}_\mu\tilde{\gamma}_\beta + \tilde{g}_{\nu\beta}\tilde{\gamma}_\mu\tilde{\gamma}_\alpha)\right], \quad (38)$$

$$S_{7/2}(p) = \frac{i}{\not{p} - M_R + i\Gamma/2}\frac{1}{36}\sum_{P_\mu P_\nu}\left(\tilde{g}_{\mu_1\nu_1}\tilde{g}_{\mu_2\nu_2}\tilde{g}_{\mu_3\nu_3}\right.$$

$$- \frac{3}{7}\tilde{g}_{\mu_1\mu_2}\tilde{g}_{\nu_1\nu_2}\tilde{g}_{\mu_3\nu_3} + \frac{3}{7}\tilde{\gamma}_{\mu_1}\tilde{\gamma}_{\nu_1}\tilde{g}_{\mu_2\nu_2}\tilde{g}_{\mu_3\nu_3}$$

$$\left. - \frac{3}{35}\tilde{\gamma}_{\mu_1}\tilde{\gamma}_{\nu_1}\tilde{g}_{\mu_2\mu_3}\tilde{g}_{\nu_2\nu_3}\right), \quad (39)$$

where

$$\tilde{g}_{\mu\nu} = -g_{\mu\nu} + \frac{p_\mu p_\nu}{M_R^2}, \quad (40)$$

$$\tilde{\gamma}_\mu = \gamma^\nu\tilde{g}_{\nu\mu} = -\gamma_\mu + \frac{p_\mu\not{p}}{M_R^2}, \quad (41)$$

and the summation over $P_\mu (P_\nu)$ in Eq. (39) goes over the $3! = 6$ possible permutations of the indices $\mu_1\mu_2\mu_3 (\nu_1\nu_2\nu_3)$. These high-spin resonance propagators and their variations have been applied with success in a number of resonance studies [17,18,26,43,44].

C. Form factors

Each hadronic vertex obtained from the Lagrangians given in Sec. II A is accompanied with a phenomenological form factor to parametrize the structure of the hadrons and to normalize the behavior of the production amplitude. Following Refs. [17,18], for intermediate baryon exchange, we take the form factor as

$$f_B(p^2) = \left(\frac{\Lambda_B^4}{\Lambda_B^4 + (p^2 - M_B^2)^2}\right)^n, \quad (42)$$

where p denotes the four-momentum of the intermediate baryon, the exponent n is taken to be 2 for all baryon exchanges, and the cutoff Λ_B is taken to be 900 MeV for all N, Λ, Σ, and Σ^* exchanges [17,18]. For the s-channel resonance exchanges, the cutoffs are treated as fit parameters. For intermediate meson exchange, we take the form factor as

$$f_M(q^2) = \left(\frac{\Lambda_M^2 - M_M^2}{\Lambda_M^2 - q^2}\right)^m, \quad (43)$$

where q represents the four-momentum of the intermediate meson, the exponent m is taken to be 2 for all meson exchanges, and M_M and Λ_M designate the mass and cutoff mass of exchanged meson M. We choose $M_\kappa = 800$ MeV, and for

other exchanged mesons, the experimental values are used for their masses. The cutoffs $\Lambda_{K^*} = 900$ MeV and $\Lambda_\kappa = 1100$ MeV are adopted in the present work, which are also taken from Ref. [18]. The cutoff Λ_K is treated as a free parameter and will be determined by a fit to the experimental differential cross section data.

Note that the gauge-invariance feature of our photoproduction amplitude is independent of the specific form of the form factors.

III. RESULTS AND DISCUSSION

As mentioned in Sec. I, the work of Ref. [18] presents so far the only detailed theoretical analysis of the most recent high-statistics differential cross section data from CLAS [9] for the $K^{*+}\Lambda$ photoproduction reaction. There, four nucleon resonances, namely $N(2000)5/2^+$, $N(2060)5/2^-$, $N(2120)3/2^-$, and $N(2190)7/2^-$, have been considered with the parameters of $N(2000)5/2^+$ and $N(2060)5/2^-$ taken from Ref. [21], the parameters of $N(2190)7/2^-$ taken from a relativistic quark model calculation [22], and the parameters of $N(2120)3/2^-$ determined by a fit to the experimental data. It was found that the $N(2120)3/2^-$ and $N(2190)7/2^-$ resonances are essential in describing the measured cross section data. The $N(2060)5/2^-$ resonance was found to have a relative small but still noticeable contribution, while the $N(2000)5/2^+$ was found to be negligible in this reaction.

In the present work, we adopt a rather different strategy than Ref. [18] for investigating the roles of nucleon resonances in the $\gamma p \rightarrow K^{*+}\Lambda$ reaction. That is, in addition to the Born term, which is composed of the t-channel K, κ, K^* exchanges, the u-channel Λ, Σ, $\Sigma^*(1385)$ exchanges, the s-channel N exchange, and the generalized contact current as illustrated in Fig. 2, we introduce the s-channel nucleon resonances as few as possible in constructing the reaction amplitudes in order to achieve a satisfactory fit to the high-statistics differential cross section data from CLAS [9]. In practice, we allow in our model all those six resonances near the $K^*\Lambda$ threshold, namely, $N(2000)5/2^+$, $N(2040)3/2^+$, $N(2060)5/2^-$, $N(2100)1/2^+$, $N(2120)3/2^-$, and $N(2190)7/2^-$. After numerous trials with the inclusion of different number of nucleon resonances and different combinations of them, we found that, if only one resonance is included, the χ^2 per data point, χ^2/N, are all larger than 3. The quality of the corresponding fit results are then found to be significantly poor. In particular, in the low-energy region one gets a nearly isotropic angular distribution in the differential cross sections and, consequently, failing to reproduce the shape of the angular distribution near the ΛK^* threshold exhibited by the CLAS data. Thus, they are treated as unacceptable fit results. If two resonances are included, it is found that there are five possible sets of resonance combinations which result in fits with $\chi^2/N \lesssim 2.18$ and these fits are visually in good agreement with the data. All these five sets require a common resonance, $N(2060)5/2^-$. The other resonance is one of the
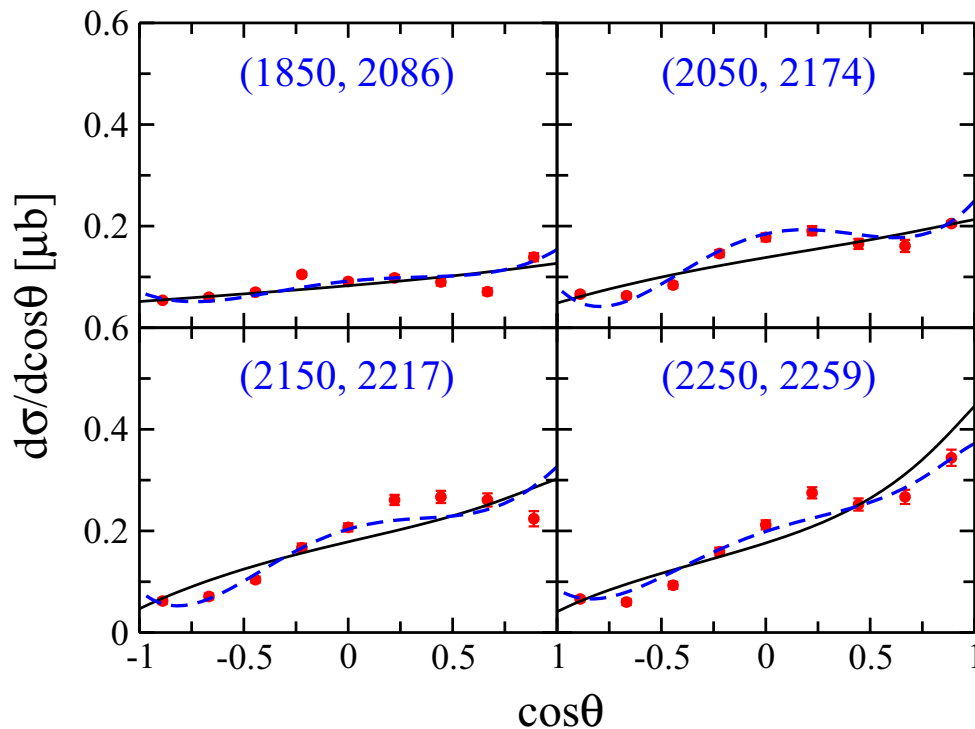

FIG. 3. Differential cross sections for $\gamma p \rightarrow K^{*+}\Lambda$ as a function of $\cos\theta$ in the center-of-mass frame in the near threshold region. The black solid lines correspond to the fit result including the $N(2000)5/2^+$ and $N(2040)3/2^+$ resonances with $\chi^2/N = 2.50$. The blue dashed lines represent the results from model V with $\chi^2/N = 2.18$. The scattered symbols are the most recent data from CLAS Collaboration [9]. The numbers in parentheses denote the photon laboratory incident energy (left number) and the total center-of-mass energy of the system (right number), in MeV.

TABLE I. Model parameters in five different fits. Here $\beta_{\Lambda K^*}$ is the branching ratio for resonance decay to ΛK^*, and $A_{1/2}$, $A_{3/2}$ are helicity amplitudes for resonance radiative decay to γp. For the definition of other parameters, see Sec. II. The stars below resonance names denote the overall status of these resonances evaluated by the most recent PDG [11]. The numbers in brackets below the resonance masses and widths represent the corresponding values estimated by the most recent PDG [11].

Model	I	II	III	IV	V
χ^2/N	1.35	1.79	1.85	2.09	2.18
$g^{(1)}_{\Sigma^*\Lambda\gamma}$	0.74 ± 0.16	-0.90 ± 0.17	-0.87 ± 0.14	-0.60 ± 0.18	-0.22 ± 0.16
Λ_K [MeV]	1000 ± 6	1019 ± 4	993 ± 7	1030 ± 3	1018 ± 4
N^* Name	$N(2060)5/2^-$	$N(2060)5/2^-$	$N(2060)5/2^-$	$N(2060)5/2^-$	$N(2060)5/2^-$
	**	**	**	**	**
M_R [MeV]	2033 ± 2	2009 ± 5	2032 ± 3	2043 ± 4	2038 ± 3
Γ_R [MeV]	65 ± 4	213 ± 20	81 ± 8	202 ± 16	77 ± 8
Λ_R [MeV]	1188 ± 20	965 ± 16	1126 ± 12	889 ± 13	981 ± 22
$\sqrt{\beta_{\Lambda K^*}}A_{1/2}$ [10^{-3} GeV$^{-1/2}$]	0.69 ± 0.06	0.03 ± 0.01	0.33 ± 0.03	0.60 ± 0.06	-0.21 ± 0.02
$\sqrt{\beta_{\Lambda K^*}}A_{3/2}$ [10^{-3} GeV$^{-1/2}$]	-1.39 ± 0.13	-0.10 ± 0.01	-1.10 ± 0.10	-1.94 ± 0.19	-1.56 ± 0.15
N^* Name	$N(2000)5/2^+$	$N(2040)3/2^+$	$N(2120)3/2^-$	$N(2190)7/2^-$	$N(2100)1/2^+$
	**	*	**	****	*
M_R [MeV]	2115 ± 22	2200 ± 62	2203 ± 9	2243 ± 6	2100 ± 15
			$[\approx 2120]$	$[2100 \sim 2200]$	$[\approx 2100]$
Γ_R [MeV]	450 ± 10	540 ± 7	433 ± 33	450 ± 33	450 ± 9
				$[300 \sim 700]$	
Λ_R [MeV]	1644 ± 21	1564 ± 36	1726 ± 58	936 ± 13	1431 ± 31
$\sqrt{\beta_{\Lambda K^*}}A_{1/2}$ [10^{-3} GeV$^{-1/2}$]	-2.87 ± 0.81	3.12 ± 0.85	4.53 ± 0.38	5.21 ± 0.33	-7.22 ± 1.40
$\sqrt{\beta_{\Lambda K^*}}A_{3/2}$ [10^{-3} GeV$^{-1/2}$]	-1.04 ± 0.29	7.87 ± 2.13	7.84 ± 0.65	3.71 ± 0.24	

$N(2000)5/2^+$, $N(2040)3/2^+$, $N(2100)1/2^+$, $N(2120)3/2^-$, and $N(2190)7/2^-$ resonances. The other combinations of two resonances all ended up in $\chi^2/N \gtrsim 2.50$, noticeably of inferior quality even with the naked eye as they fail to reproduce the shape of the measured angular distribution near threshold. Hence, they are not considered as acceptable fit results. A comparison of the fit results with two resonances, one with $\chi^2/N = 2.18$ (accepted result corresponding to model V as it will be discussed later) and another with $\chi^2/N = 2.50$ (unaccepted result with the resonances $N(2000)5/2^+$ and $N(2040)3/2^+$), is shown in Fig. 3. The difference in the fit quality is clearly seen even with the naked eye. Now, if three resonances are considered, the χ^2/N improves only slightly by less than 12% compared with that with two resonances. Therefore, in the present work we do not pursue the analysis with three or more resonances further. This will be postponed until the data for spin observables become also available. These will impose more stringent constraints on the resonance contents which, in turn, will restricts the number of possible resonance combinations with three or more resonances. With this in mind, we conclude that one needs *at least* two resonances to obtain a reasonable fit of the cross section data for $\gamma p \to K^{*+}\Lambda$ in the present approach.

We now turn to the discussion of the details of our analysis of the data with two nucleon resonances included. As mentioned above, in this case there are five different sets of the resonance combination which result in fits describing the differential cross section data of K^{*+} photoproduction reaction satisfactorily according to our criterium of $\chi^2/N < 2.5$. The fitted values of all the adjustable parameters in those five models are listed in Table I. There, the stars below the resonance names denote the overall status of these resonances

evaluated by the most recent review by the PDG [11], and the numbers in brackets below the resonance masses and widths represent the corresponding estimates given by the PDG. The uncertainties in the resulting parameters are estimates arising from the uncertainties (error bars) associated with the fitted experimental differential cross section data points. For each resonance, apart from its mass, total width, and cutoff parameter in the form factor, the table also shows the corresponding reduced helicity amplitudes $\sqrt{\beta_{\Lambda K^*}}A_j$, where $\beta_{\Lambda K^*}$ denotes the branching ratio to the decay channel ΛK^* and A_j stands for the helicity amplitude with spin j. We mention that only the product of these two quantities can be well constrained in the present work as the s-channel (resonance) amplitudes are sensitive only to the product of the hadronic and electromagnetic coupling constants, a feature common to single-channel calculations. Following Ref. [26], here we have assumed a radiative branching ratio of $\beta_{p\gamma} = 0.2\%$ for all the resonances to calculate the corresponding helicity amplitudes from the associated product of the hadronic and electromagnetic coupling constants. It is seen from Table I that the coupling $g^{(1)}_{\Sigma^*\Lambda\gamma}$ varies much from one model to another. This is simply because the u-channel $\Sigma^*(1385)$ exchange has negligible contribution to the reaction $\gamma p \to K^{*+}\Lambda$ (cf. Figs. 5 and 6 discussed later in this section). The fitted values of Λ_K, the cutoff parameter in the K-meson exchange contribution, are very close to each other in models I–V—they are all around 1.0 GeV. This value is determined mainly by the data in the high-energy region, where the K meson exchange dominates the whole amplitude of this reaction (cf. Figs. 5 and 6). The fitted values of the mass of $N(2060)5/2^-$ from various models are also very close to each other, while those of its decay width are not. In
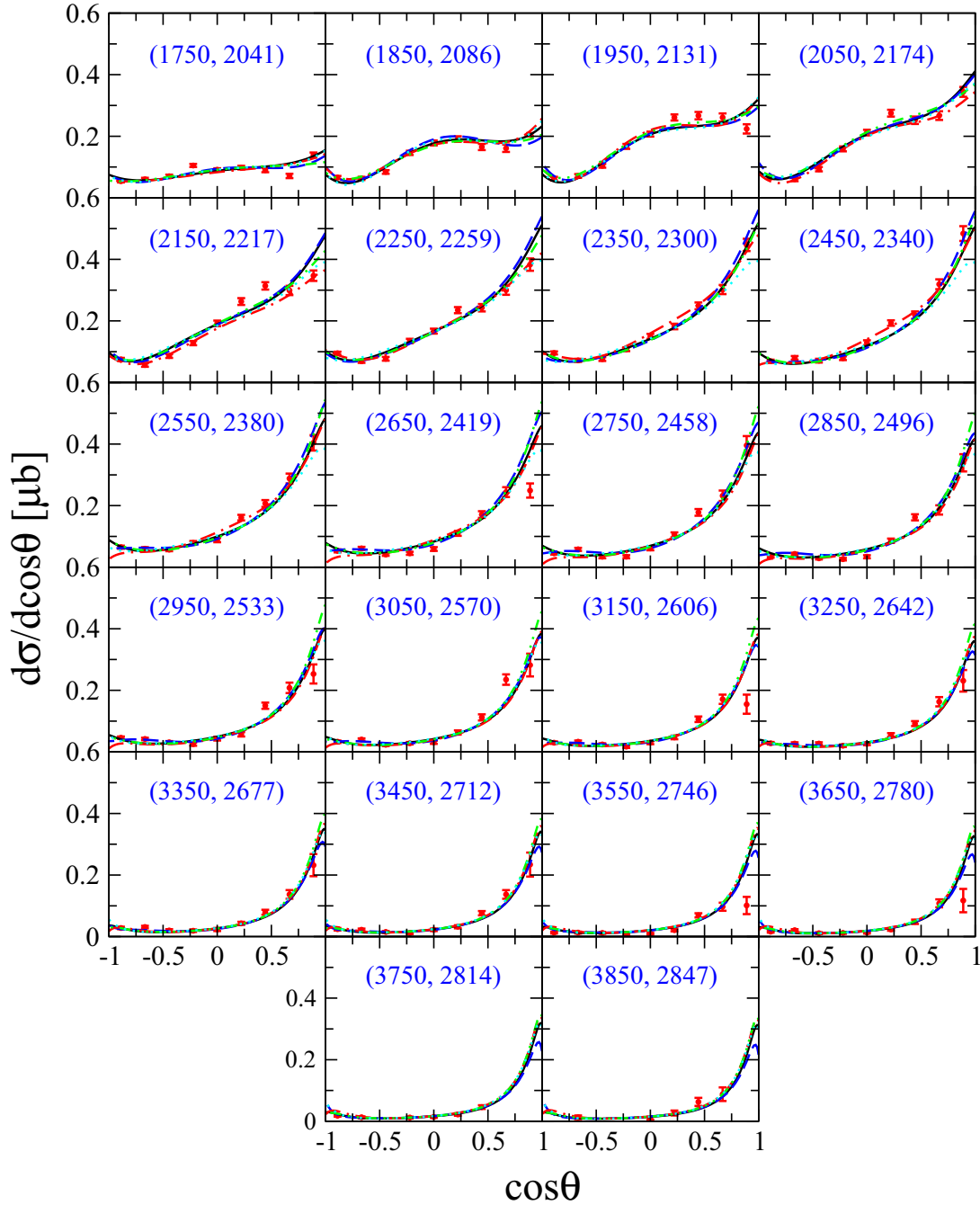
FIG. 4. Differential cross sections for $\gamma p \rightarrow K^{*+}\Lambda$ as a function of $\cos\theta$ in the center-of-mass from models I (black solid lines), II (green dash-double-dotted lines), III (black solid lines), IV (red dash-dotted lines), and V (cyan dotted lines). The scattered symbols denote the CLAS data [9]. The photon incident energy binning is 100 MeV. The numbers in parentheses denote the centroid value of the photon laboratory incident energy (left number) and the corresponding total center-of-mass energy of the system (right number), in MeV.

each of the models I–V, the value of the fitted mass of the other resonance is compatible with that quoted in PDG [11]. The fit result for the width of the four-star $N(2190)7/2^-$ is compatible with the PDG estimate which has a large range. The widths of the $N(2000)5/2^+$, $N(2040)3/2^+$, $N(2120)3/2^-$, and $N(2100)1/2^+$ resonances obtained in the present work are somewhat larger than those obtained in the other analyses listed in the PDG. We note that the reduced helicity amplitudes for $N(2060)5/2^-$ corresponding to model II are much smaller

than those corresponding to the other models. This is caused by the smaller value of the resulting resonance mass of 2009 ± 5 MeV for model II, leading to a much smaller branching ratio $\beta_{\Lambda K^*}$. Note that the $R \rightarrow \Lambda K^*$ decay threshold is 2007 MeV; thus, for model II, the $N(2060)5/2^-$ resonance is only 2 MeV above the threshold. We will discuss further details below in connection with the differential cross section results shown in Figs. 4 and 5 and the total cross section results shown in Fig. 6.
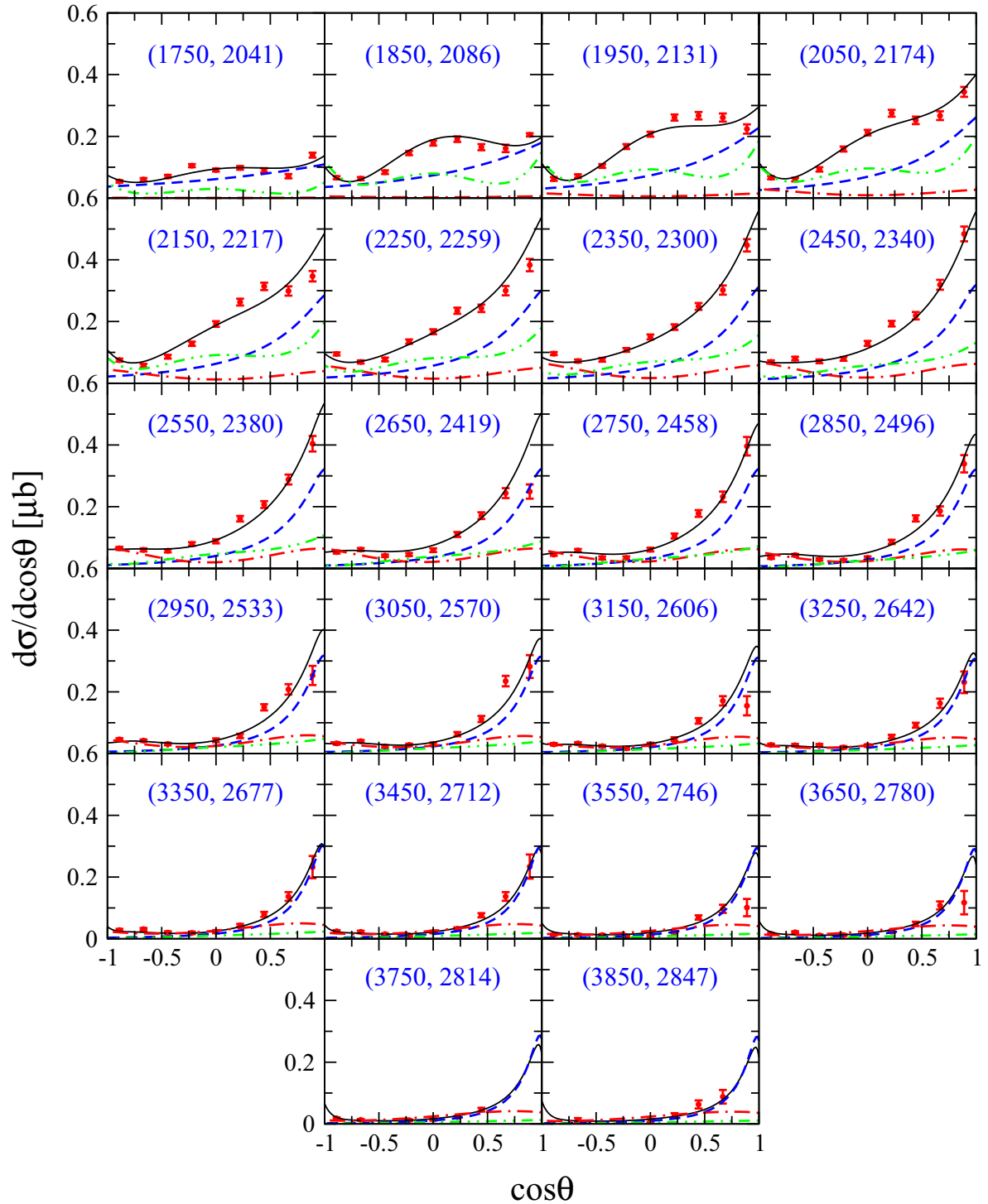
FIG. 5. Differential cross sections for $\gamma p \to K^{*+}\Lambda$ as a function of $\cos\theta$ in the center of mass from model I (black solid lines). The scattered symbols denote the CLAS data [9]. The blue dashed, green dash-double-dotted, and magenta dash-dotted lines represent the individual contributions from K, $N(2060)5/2^-$, and $N(2000)5/2^+$ exchanges, respectively. The photon incident energy binning is 100 MeV. The numbers in parentheses denote the centroid value of the photon laboratory incident energy (left number) and the corresponding total center-of-mass energy of the system (right number), in MeV.

The results for differential cross sections corresponding to the model parameters listed in Table I are shown in Fig. 4, where the black solid lines, green dash-double-dotted lines, black solid lines, red dash-dotted lines, and cyan dotted lines represent the results from models I–V, respectively. One sees that the overall description of the CLAS high-statistics angular distribution data is fairly satisfactory in all of the five models. In particular, the angular dependence of the differential cross
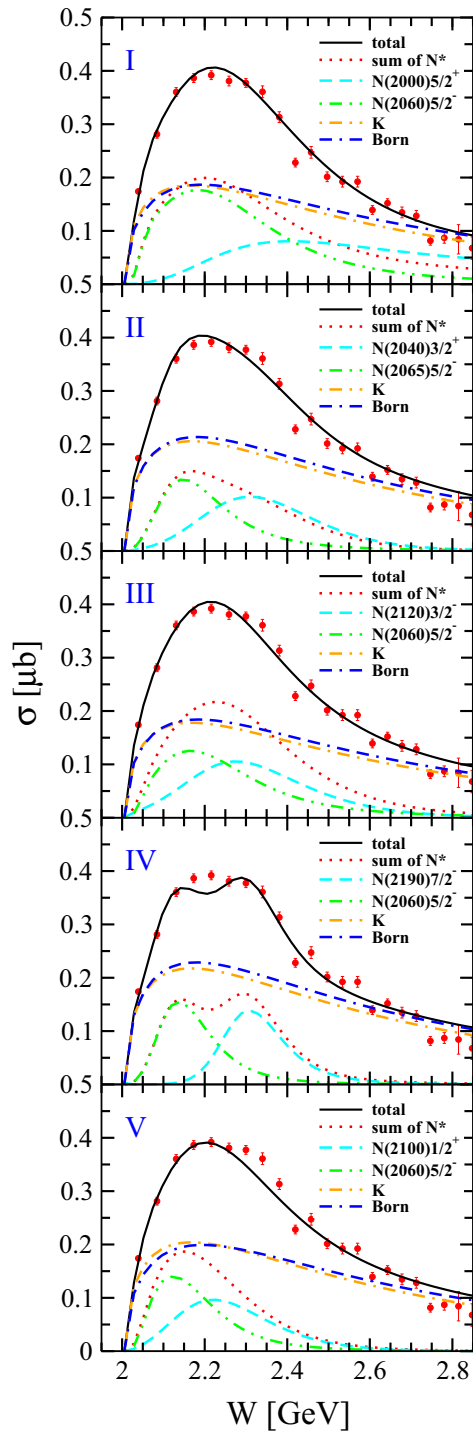
FIG. 6. Total cross sections with individual (resonance, Born term, K) contributions for $\gamma p \to K^{*+}\Lambda$. The panels from top to bottom correspond to the results of modes I–V, as indicated. The data are from CLAS [9] but not included in the fit.

sections near the ΛK^* threshold is qualitatively in good agreement with the data, much better than the description of Ref. [18] (cf. Fig. 1). This is because in all our models I–V, there is a significant contribution from the $N(2060)5/2^-$ resonance in the low-energy region that is responsible for

reproducing the observed shape of the angular distribution through an interference with the large K-meson exchange contribution near the ΛK^* threshold (cf. Fig. 5). In contrast, Ref. [18] has a rather small contribution of $N(2060)5/2^-$ and clear discrepancies are seen in its description of the near-threshold differential cross section data (cf. Fig. 1). This consideration explains why the mass of $N(2060)5/2^-$ is fairly well constrained, as can be seen from the resulting values in Table I for models I–V. Figure 5 shows the individual contributions in model I, where the black solid lines correspond to the total contribution (coherent sum of all the individual contributions), the blue dashed lines represent the contribution from the t-channel K-meson exchange, the green dash-double-dotted lines indicate the s-channel $N(2060)5/2^-$ exchange, and the magenta dash-dotted lines denote the contribution from the s-channel $N(2000)5/2^+$ resonance exchange. The contributions from the other terms are too small to be clearly seen with the scale used, and thus they are not plotted. We note that the contributions other than the $N(2060)5/2^-$ resonance and K-meson exchange are practically negligible in the low-energy region. The contributions from individual terms in models I–V as a function of energy can be better seen in the total cross section (cf. Fig. 6). In Fig. 5, one sees that the K-meson exchange is very important in the whole energy region considered. In particular, it plays a crucial role in reproducing the observed forward-peaked angular distribution at higher energies. This is a general feature observed in many reactions at high energies, where the t-channel mechanism accounts for the behavior of the cross section at small t. This explains why the cutoff parameter values (Λ_K), which is the only adjustable parameter for K-meson exchange, are close to each other in all of our models I–V. In other words, our K-meson exchange contribution—which practically exhausts the calculated non-resonant background in the entire energy region—is largely constrained by the data at high energies. This leads to a much more unambiguous determination of the resonance contributions in the present model. On the other hand, it is also very interesting to see how the Regge trajectory description of the present reaction would affect the strong angular dependence at very forward angles at high energies exhibited by the K-meson exchange mechanism where no data exist due to the limitations in the forward-angle acceptance of the CLAS detector [9]. The gauge-invariant dynamical Regge approach put forward in Ref. [16] seems well suited for this purpose; however, this is left for a future investigation.

Before we leave the discussion of the differential cross section results, we mention that although the present calculation describes the differential cross section data quite well overall and much better than any of the earlier calculations, the agreement with the data is not perfect. Indeed, the details of the observed angular behavior at $W = 2.217$ GeV is not quite described by any of our models I–V. Also, our models show a slight tendency to miss the data at the neighboring energies of $W = 2.174$ and 2.259 GeV. As mentioned before, the inclusion of one more resonance did not help improve the fit quality much. Further investigation is required here.

Figure 6 shows the predicted total cross sections (black solid line) together with the individual contributions from the K exchange (orange dash-dotted line), Born term (blue

double-dash-dotted line), and the resonances (green dash-double-dotted line and cyan dashed line) obtained by integrating the corresponding results for differential cross sections from our models I–V. We recall that the Born term consists of the coherent sum of all the contributions other than the s-channel resonance exchanges, i.e., the coherent sum of the s-channel N exchange; the t-channel K, K^*, and κ exchanges; the u-channel Λ, Σ, and $\Sigma^*(1385)$ exchanges; and the generalized contact current. Note that the total cross section data are not included in our fits. In this regard, it should be emphasized that the CLAS total cross section data have been obtained by integrating the measured differential cross sections and suffer from the limited forward-angle acceptance of the CLAS detector [9], especially at high energies where the cross section exhibits a strong angular dependence at very forward angles (cf. Figs. 4 and 5). The lack of differential cross section data at very forward angles and high energies reflects in less accurate CLAS total cross section data at these energies. Hence, caution must be exercised when confronting these data with theoretical predictions. One sees from Fig. 6 that in all of our models I–V, the predicted total cross sections are in fairly good agreement with the data over the entire energy region considered, with one exception that, in model IV, the predicted total cross sections exhibit a small valley structure around $W \sim 2.2$ GeV; we come back to this point later. The K meson exchange is seen to play an important role in the whole energy region, especially at high energies. Its contribution in all of the models I–V is more or less similar to each other, as the only adjustable parameter for K meson exchange, the cutoff mass Λ_K in the form factor, is constrained by the differential cross section data at high energies, where this contribution practically dominates this observable. We observe that our total cross section predictions exhibit a slight tendency to overestimate the data at very high energies, although the data are much less accurate and may suffer from the limitations in the CLAS detector acceptance as mentioned above. Nevertheless, as mentioned previously in connection to the discussion of the differential cross sections, it would be interesting to see how the Regge trajectory description of the present reaction along the lines suggested in Ref. [16] would affect the cross section at these high energies. The contributions from the nonresonant terms other than the K-meson exchange are negligible, as can be seen by comparing the Born term (red dash-double-dotted line) with the K exchange (blue short dashed line) contribution. The negligible contribution of the u-channel $\Sigma^*(1385)$ exchange—which is a part of the nonresonant term—explains why the coupling $g^{(1)}_{\Sigma^*\Lambda\gamma}$ varies so much from one model to another in Table I with roughly similar fit qualities.

The broad bump exhibited by the total cross section is caused by the coherent sum of the considered two resonances and K-meson exchange contributions. In all of the models I–V, the sharp rise of the cross section from the threshold up to $W \sim 2.15$ GeV is caused by the K-meson exchange and $N(2060)5/2^-$ resonance. The other resonance contributes mostly at higher energies. These are better seen in Fig. 7, where the effects of the $N(2060)5/2^-$ and $N(2000)5/2^+$ on the total cross section are shown by switching off these resonances one at a time. One clearly sees that the K-meson
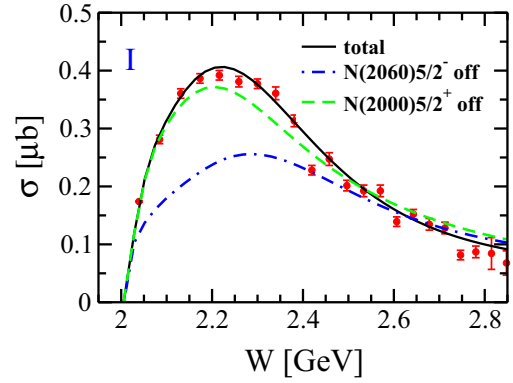

FIG. 7. Same as in Fig. 6 for model I. The blue dash-dotted line corresponds to the results with resonance $N(2060)5/2^-$ switched off, while the green dashed line to those with $N(2000)5/2^+$ switched off. The black solid line is the results of model I shown in Fig. 6.

exchange is responsible for the sharp raise of the total cross section right from the threshold followed by the buildup due to $N(2060)5/2^-$ as the energy increases up to $W \sim 2.1$ GeV. In Ref. [18], the differential cross section near the ΛK^* threshold is not well described (cf. Fig. 1), and consequently, the total cross section in this energy region is, to some extent, underestimated. There, the broad bump is mainly described by the sum of the contributions of $N(2120)3/2^-$, $N(2060)5/2^-$, and $N(2190)7/2^-$, and the sharp rise of the total cross section from the threshold is dominantly caused by the combination of the contributions from the $N(2120)3/2^-$ resonance and the Born term. We mention that the contribution of the K meson exchange in our models is a little bit different from that in Ref. [18], not only because the cutoff mass Λ_K is fitted to be around 1.0 GeV in our model while it is fixed to be 1.1 GeV in Ref. [18], but also due to the pseudovector coupling chosen in our models for the ΛNK vertex [see Eq. (23)] in contrast to the pseudoscalar coupling adopted in Ref. [18].

We now come back to the issue of the dip structure exhibited by the total cross section result of model IV, which is caused by the interference of the $N(2060)5/2^+$ and $N(2190)7/2^-$
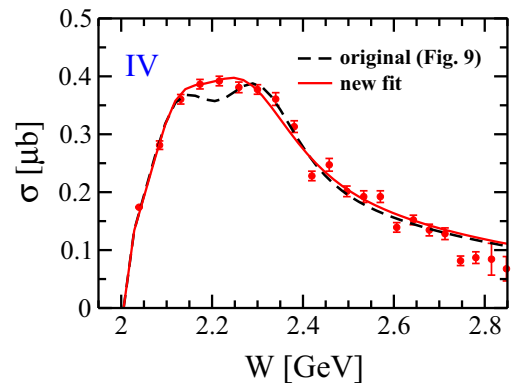

FIG. 8. Same as in Fig. 6 for model IV, except that it has been artificially forced to better reproduce the measured differential cross section at $W = 2.217$ GeV (red solid line). The black dashed line is the results of model IV shown in Fig. 6.
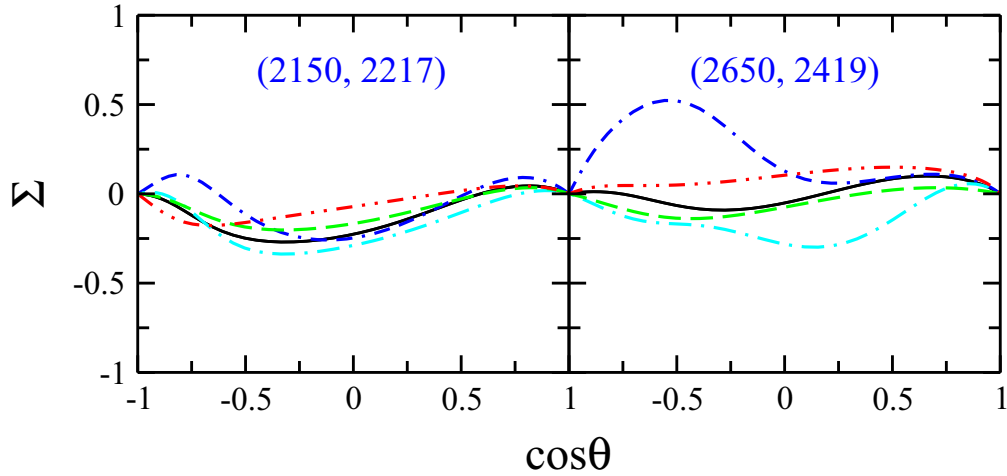
FIG. 9. Photon beam asymmetries as functions of cosine of the K^* emission angle θ in the center-of-mass system at two energies for the $\gamma p \to K^{*+}\Lambda$ reaction. The numbers in parentheses denote the photon laboratory incident energy (left number) and the total center-of-mass energy of the system (right number), in MeV. The blue double-dash-dotted curve, green dashed curve, black solid curve, cyan dash-dotted curve, and orange dash-double-dotted curve represent the predictions corresponding to the models I–V, respectively.

resonances as can be seen from Fig. 6. Clearly, the data do not show such a structure. A careful inspection of the differential cross section fit results of model IV reveals that this structure is due to the model not being able to quite describe the measured differential cross section data at one energy, namely, at $W = 2.217$ GeV. We note that, actually, not only model IV, but all the other models are unable to quite reproduce the angular behavior exhibited by the data at this energy. The relevant difference between the results of model IV and the other models that causes the valley structure in model IV is that model IV underpredicts the data in the angular region of $0 \lesssim \cos\theta \lesssim 0.5$, while the other models also underpredict in this angular region but overpredict for other angles. As a result, the total cross section predictions for other models agree with the data but it is underpredicted by model IV at this energy. In fact, if one is forced to describe the differential cross section better at $W = 2.217$ GeV (at the expenses of a slightly deteriorating description for the neighboring energies), the dip

structure in the prediction of model IV disappears completely, as illustrated in Fig. 8.

As can be seen in Figs. 4 and 5 and as has been discussed above, the models I–V describe the most recent CLAS data on the differential cross sections for K^{*+} photoproduction fairly well overall and with similar fit qualities in the full energy-range considered. However, they exhibit quite different resonance contents, as indicated in Table I and clearly seen in the total cross section predictions shown in Fig. 6. By now, it is a well-known fact that the cross section data alone (even with high statistics) do not impose enough stringent constraints on the fits to pin down the model parameters, especially on the resonance contents and associated resonance parameters. Such a feature has also been found and discussed in Ref. [39] in a study of η' photoproduction. One expects that the spin observables may be more sensitive to the dynamical contents of different models. In Figs. 9–11, we show the predictions of the photon beam asymmetry (Σ), target nucleon asymmetry (T),
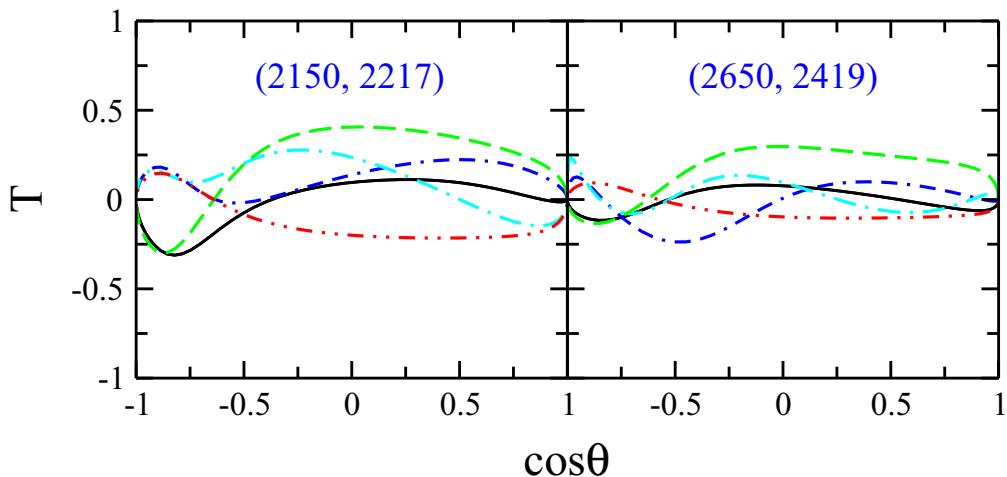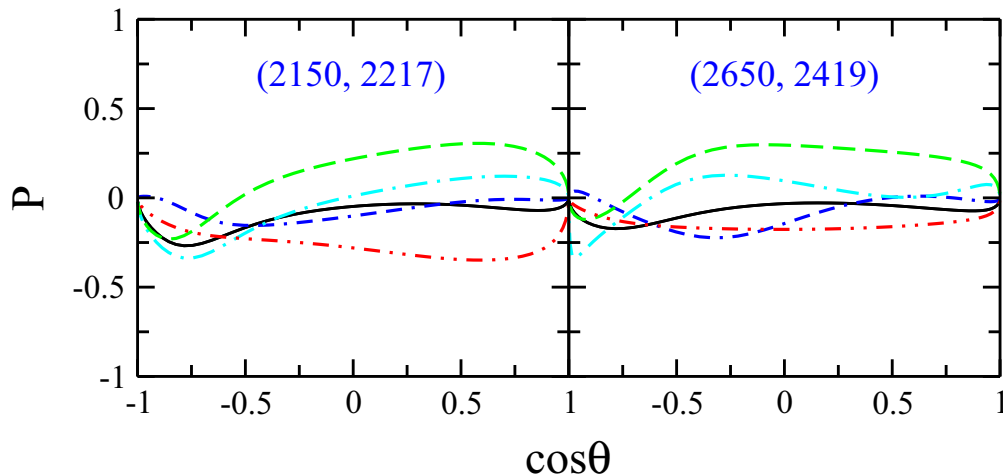

FIG. 10. Same as in Fig. 9 for target nucleon asymmetries.

FIG. 11. Same as in Fig. 9 for recoil Λ asymmetries.

and recoil Λ asymmetry (P) corresponding to our models I–V. As we can see, unlike the cross sections, the predictions for spin observables vary considerably among different models. For energies where the photon beam asymmetry is less sensitive to the models, the target nucleon asymmetry and the recoil Λ asymmetry are quite sensitive, and vice versa. Therefore, overall, a combined analysis of the data of these spin observables is expected to impose much more stringent constraints on the resonance contents and help better determine the model parameters for $\gamma p \rightarrow K^{*+}\Lambda$. We hope that these spin observables can be measured in experiments in the near future.

IV. SUMMARY AND CONCLUSION

In the present work, we have analyzed the most recent high-statistic cross section data reported by the CLAS Collaboration for the $\gamma p \rightarrow K^{*+}\Lambda$ reaction [9]. The analysis has been based on an effective Lagrangian approach in the tree-level approximation. Apart from the t-channel K, κ, K^* exchanges, the s-channel nucleon (N) exchange, the u-channel Λ, Σ, $\Sigma^*(1385)$ exchanges, and the generalized contact current, the contributions from the near-threshold nucleon resonances in the s channel have been also taken into account in constructing the reaction amplitude. The generalized contact current introduced in the present work ensures that the reaction amplitude in our model is fully gauge invariant as it obeys the generalized Ward-Takahashi identity [23–26].

It is found that to obtain a satisfactory description of the high-statistics differential cross section data from CLAS, *at least* two nucleon resonances should be included in the s-channel interaction diagrams. Furthermore, we have found five distinct sets of resonances that describe these data with similar accuracies in the whole energy range of 1.75 GeV $\leqslant E_\gamma \leqslant$ 3.85 GeV. One of these two resonances, common to all five sets, is the $N(2060)5/2^-$; the other resonance in each of the five sets is $N(2000)5/2^+$, $N(2040)3/2^+$, $N(2100)1/2^+$, $N(2120)3/2^-$, and $N(2190)7/2^-$, respectively. The differential cross section data near the ΛK^* threshold is for the first time described quite

satisfactorily. The resulting resonance masses are compatible with those advocated by the Particle Data Group (PDG) [11]. Although the CLAS total cross section data—which are obtained by integrating the measured differential cross sections—may suffer from the limited angular acceptance of the CLAS detector for forward angles, the predicted total cross sections are in good agreement with these data.

It is shown that, together with the K-meson exchange, the $N(2060)5/2^-$ resonance practically determine the dynamics of the $\gamma p \rightarrow K^{*+}\Lambda$ reaction in the low-energy region in the present model. In particular, they are responsible for the observed shape of the angular distribution and for the sharp raise of the total cross section from the threshold up to $W \sim 2.1$ GeV. The other resonance, in each of the five sets, contribute significantly at higher energies. The K-meson exchange provides a very significant contribution to the cross sections in the entire energy range considered, especially at high energies where it dominates the cross section to a large extent, while the contributions from the other nonresonant terms are found to be negligible.

The predicted photon beam asymmetry, target nucleon asymmetry, and recoil Λ asymmetry are found to vary considerably from one model to another, indicating their sensitivity to the details of the models, in particular, to the different resonance contents that cannot be distinguished by the cross section alone. It is expected that the data for these spin observables would impose more stringent constraints on the models than the cross sections and help understand better the reaction mechanism and determine better the resonance contents and associated resonance parameters in the $\gamma p \rightarrow K^{*+}\Lambda$ reaction. We hope that these data can be measured in experiments in the near future.

We should also mention that although the present calculation describes the differential cross section data quite well overall and much better than any of the earlier calculations, the agreement with the data is not perfect. In particular, the details of the observed angular behavior at $W = 2.217$ GeV is not quite described by any of our models I–V. As mentioned in Sec. III, the inclusion of one more resonance does not help

improve much the fit quality. Further investigation is required here.

[1] N. Isgur and G. Karl, Phys. Rev. D **18**, 4187 (1978).
[2] S. Capstick and N. Isgur, Phys. Rev. D **34**, 2809 (1986).
[3] U. Löring, B. C. Metsch, and H. R. Petry, Eur. Phys. J. A **10**, 395 (2001).
[4] R. Koniuk and N. Isgur, Phys. Rev. Lett. **44**, 845 (1980).
[5] R. G. Edwards, N. Mathur, D. G. Richards, and S. J. Wallace (Hadron Spectrum Collaboration), Phys. Rev. D **87**, 054506 (2013).
[6] G. P. Engel, C. B. Lang, D. Mohler, and A. Schäfer (BGR [Bern-Graz-Regensburg] Collaboration), Phys. Rev. D **87**, 074504 (2013).
[7] L. Guo and D. P. Weygand (CLAS Collaboration), arXiv:hep-ex/0601010.
[8] K. Hicks, D. Keller, and W. Tang, AIP Conf. Proc. **1374**, 177 (2011).
[9] W. Tang *et al.* (CLAS Collaboration), Phys. Rev. C **87**, 065204 (2013).
[10] P. Mattione (CLAS Collaboration), Int. J. Mod. Phys. Conf. Ser. **26**, 1460101 (2014).
[11] C. Patrignani *et al.* (Particle Data Group), Chin. Phys. C **40**, 100001 (2016).
[12] Y. Oh and H. Kim, Phys. Rev. C **73**, 065202 (2006).
[13] Y. Oh and H. Kim, Phys. Rev. C **74**, 015208 (2006).
[14] S. Ozaki, H. Nagahiro, and A. Hosaka, Phys. Rev. C **81**, 035206 (2010).
[15] M. Guidal, J.-M. Laget, and M. Vanderhaghen, Nucl. Phys. A **627**, 645 (1997).
[16] H. Haberzettl, X.-Y. Wang, and J. He, Phys. Rev. C **92**, 055503 (2015).
[17] S.-H. Kim, S.-i. Nam, Y. Oh, and H.-C. Kim, Phys. Rev. D **84**, 114023 (2011).
[18] S.-H. Kim, A. Hosaka, and H.-C. Kim, Phys. Rev. D **90**, 014021 (2014).
[19] B.-G. Yu, Y. Oh, and K.-J. Kong, Phys. Rev. D **95**, 074034 (2017).
[20] X.-Y. Wang and J. He, Phys. Rev. C **93**, 035202 (2016).
[21] A. V. Anisovich, R. Beck, E. Klempt, V. A. Nikonov, A. V. Sarantsev, and U. Thoma, Eur. Phys. J. A **49**, 67 (2013).
[22] S. Capstick, Phys. Rev. D **46**, 2864 (1992).
[23] H. Haberzettl, Phys. Rec. C **56**, 2041 (1997).
[24] H. Haberzettl, K. Nakayama, and S. Krewald, Phys. Rev. C **74**, 045202 (2006).
[25] F. Huang, M. Döring, H. Haberzettl, J. Haidenbauer, C. Hanhart, S. Krewald, U.-G. Meißner, and K. Nakayama, Phys. Rev. C **85**, 054003 (2012).
[26] F. Huang, H. Haberzettl, and K. Nakayama, Phys. Rev. C **87**, 054004 (2013).
[27] X. Cao, V. Shklyar, and H. Lenske, Phys. Rev. C **88**, 055204 (2013).
[28] A. V. Anisovich, R. Beck, E. Klempt, V. A. Nikonov, A. V. Sarantsev, and U. Thoma, Eur. Phys. J. A **48**, 15 (2012).
[29] D. Rönchen, M. Döring, F. Huang, H. Haberzettl, J. Haidenbauer, C. Hanhart, S. Krewald, U.-G. Meißner, and K. Nakayama, Eur. Phys. J. A **49**, 44 (2013).
[30] H. Kamano, S. X. Nakamura, T.-S. H. Lee, and T. Sato, Phys. Rev. C **92**, 025205 (2015).
[31] C. Fernandez-Ramirez, I. V. Danilkin, D. M. Manley, V. Mathieu, and A. P. Szczepaniak, Phys. Rev. D **93**, 034029 (2016).
[32] S. D. Drell and T. D. Lee, Phys. Rev. D **5**, 1738 (1972).
[33] D. Black, M. Harada, and J. Schechter, Phys. Rev. Lett. **88**, 181603 (2002).
[34] H. Garcilazo and E. Moya de Guerra, Nucl. Phys. A **562**, 521 (1993).
[35] K. Nakayama, Y. Oh, and H. Haberzettl, Phys. Rev. C **74**, 035205 (2006).
[36] J. Haidenbauer, S. Petschauer, N. Kaiser, U.-G. Meißner, A. Nogga, and W. Weise, Nucl. Phys. A **915**, 24 (2013).
[37] J. J. Swart, Rev. Mod. Phys. **35**, 916 (1963).
[38] V. G. J. Stoks and T. A. Rijken, Phys. Rev. C **59**, 3009 (1999).
[39] K. Nakayama and H. Haberzettl, Phys. Rev. C **73**, 045211 (2006).
[40] R. E. Behrends and C. Fronsdal, Phys. Rev. **106**, 345 (1957).
[41] C. Fronsdal, Supp. Nuovo Cimento **9**, 416 (1958).
[42] J. J. Zhu and M. L. Yan, arXiv:hep-ph/9903349.
[43] J. K. Man, Y. Oh, and K. Nakayama, Phys. Rev. C **83**, 055201 (2011).
[44] B. C. Jackson, Y. Oh, H. Haberzettl, and K. Nakayama, Phys. Rev. C **91**, 065208 (2015).